

## Article

# Web-Crippling Capacity of High Performance Cold-Formed Lipped Steel Sections Subjected to Elevated Temperature

Gunasekaran Jayakumar <sup>1,2</sup>, Tattukolla Kiran <sup>1</sup> , Anand Nammalvar <sup>1,\*</sup>, Tilak Prasad Sah <sup>3</sup>,  
Mervin Ealiyas Mathews <sup>4</sup> , M. Anbarasu <sup>5,\*</sup>  and A. R. Dar <sup>6</sup>

<sup>1</sup> Department of Civil Engineering, Karunya Institute of Technology and Sciences, Coimbatore 641114, India

<sup>2</sup> Department of Civil Engineering, Sri Krishna College of Technology, Coimbatore 641042, India

<sup>3</sup> Centre of Infrastructural Monitoring and Protection, Curtin University, Perth 6102, Australia

<sup>4</sup> L&T Edu Tech, Larsen & Toubro Limited, Chennai 600116, India

<sup>5</sup> Department of Civil Engineering, Government College of Engineering, Salem 636011, India

<sup>6</sup> Department of Civil Engineering, National Institute of Technology, Srinagar, Srinagar 190006, India

\* Correspondence: nanand@karunya.edu (A.N.); anbarasu@gcesalem.edu.in (M.A.)

**Abstract:** High-performance steel has emerged as an advanced structural material in the construction practice of industrial buildings, due to its excellent properties. However, fire poses a significant threat to cold-formed steel structures, as they are prone to deform and buckle under the exposure, potentially leading to building collapse. This study aimed to evaluate the post-fire web-crippling behaviour of high performance CFS sections for End Two Flange (ETF) and Interior Two Flange (ITF) load cases. Two types of specimens were used: CFS webs without holes and CFS webs with circular holes. All test specimens were heated according to the ISO 834 standard fire curve and were subsequently cooled by air or water. A total of 52 specimens (ambient and post-fire) were tested under ETF and ITF load conditions. The load-deflection behaviour and failure modes were evaluated through experimental and numerical analysis. Finite element modelling was used to compare the load-deflection behaviour and failure modes of CFS members with experimental results. The experimental results indicate that the web load-carrying capacity of the high-performance steel member decreases drastically as the heating duration increases. Furthermore, the ITF load case specimens exhibited a lower strength loss than the ETF load case specimens at elevated temperatures. There was an excellent agreement between the experimental and FEM results in terms of the load-carrying capacity and failure modes of high performance CFS.

**Keywords:** high performance cold formed steel; web-crippling behaviour; elevated temperature; circular web openings; finite element analysis



**Citation:** Jayakumar, G.; Kiran, T.; Nammalvar, A.; Prasad Sah, T.; Mathews, M.E.; Anbarasu, M.; Dar, A.R. Web-Crippling Capacity of High Performance Cold-Formed Lipped Steel Sections Subjected to Elevated Temperature. *Buildings* **2023**, *13*, 2436. <https://doi.org/10.3390/buildings13102436>

Academic Editors: Mohammad Adil Dar and Seyed Mohammad Mojtabaei

Received: 26 June 2023

Revised: 7 September 2023

Accepted: 21 September 2023

Published: 25 September 2023



**Copyright:** © 2023 by the authors. Licensee MDPI, Basel, Switzerland. This article is an open access article distributed under the terms and conditions of the Creative Commons Attribution (CC BY) license (<https://creativecommons.org/licenses/by/4.0/>).

## 1. Introduction

In recent times, high-performance cold-formed steel (CFS) structures have become increasingly popular in construction practices due to their strength, durability, and versatility of construction. This is primarily due to the several advantages offered by high-performance CFS, including the use of light-gauge sections, innovative profiles of preferable size, high strength-to-weight ratio, requirement of less manpower, and ease of transportation and assembly [1]. Moreover, in various countries, the design standards and guidelines for CFS elements have been well established, thereby increasing the demand for CFS members in construction practices and for other applications [2].

Additionally, high-performance CFS is used as a flexural member for roof purlins and floor joists, among other applications. When subjected to a concentrated force, the web portion of the section may experience localized failure, which is represented as a web-crippling failure [3]. The web-crippling failure is also categorized into four different load categories, namely Interior-One-Flange loading (IOF), End-One-Flange loading (EOF), Interior-Two-Flange loading (ITF), and End-Two-Flange loading (ETF) [4]. Additionally,

each category is tested under fastened and unfastened stiffened flange conditions [5]. Figure 1 shows the year-wise progress of the research work in the web-crippling studies (experimental and numerical).

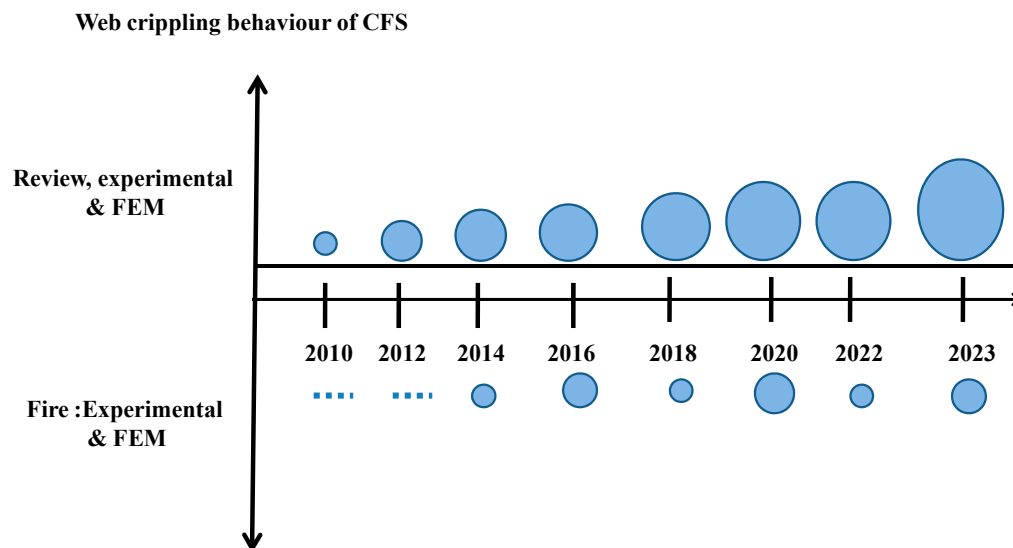


**Figure 1.** Past research works on web-crippling of high performance CFS exposed to ambient and high temperature.

Natalia Degtyareva et al. (2021) conducted an experimental investigation on the web-crippling behaviour of CFS-C channels under ETF and ITF load conditions. The study was carried out with and without slotted web sections, and they proposed new web-crippling design equations to calculate reduced web-crippling capacities [6]. Lavan Sundararajah et al. (2017) performed an experimental and numerical investigation on the web-crippling behaviour of high strength CFS beams under EOF and IOF loading. They have conducted a detailed parameter and numerical studies by varying the section geometry and mechanical properties. The research resulted in the development of numerical equations for yield loads and elastic buckling of CFS sections based on the guidelines of direct strength method (DSM) [7].

Elilarasi Kanthasamy et al. (2022) conducted a detailed experimental and numerical analysis on high strength CFS unlippped sections under EOF conditions. They performed a detailed parametric study and developed 243 FEM models that were compared with experimental results. The study revealed that the experimental and numerical results showed a strong correlation [8]. Zhiyuan Fang et al. (2022) conducted a numerical simulation on CFS stainless steel sections with web holes under IOF loading conditions. They developed a total of 1728 numerical models and performed design guidelines and reliability analysis. The study reported that the developed design equations accurately predicted the experimental results [9]. Hancock et al. [10] developed Finite Strip Method (FSM) for buckling analysis of thin sections subjected to different support and boundary conditions. Nguyen et al. [11,12] determined deflections and membrane stresses based on the theory of FSM which is applied in buckling analysis.

From the comprehensive literature analysis, it is evident that the previous researchers [3–9] have conducted extensive investigations and numerical studies. They have also performed a detailed parametric study by varying section profiles, steel grades, material properties, support condition, and loading conditions. Considering the design aspect on the web-crippling behaviour of CFS, researchers have developed guidelines by following the available design codes [13–15]. Additionally, DSM were developed for different loading conditions using generalized equations, considering buckling load and yield load [16,17].

Fire is a hazardous factor that can cause significant damage to CFS structures. When exposed to fire, CFS can lose its physical and mechanical properties, as well as stiffness, ultimately leading to structural collapse [18]. Krishanu Roy et al. (2022) conducted a

real-time fire experiment on a CFS truss structure and found that a critical temperature of 622.5 °C led to the collapse of the roof truss system with inward asymmetrical buckling [19]. Ali Nadjai et al. (2022) studied a real-time travelling fire experiment on open ventilation of steel structures and reported that the steel structural elements become unstable during the event of fire, leading to global failure. The travelling fire conditions pose a risk for steel structures in the future [20].

The literature review revealed that an extensive investigation has been conducted on the numerical behaviour of carbon CFS elements at elevated temperatures [21]. Researchers have developed various numerical models to analyse the axial and flexural behaviour of CFS elements under elevated temperature conditions [22–24]. Yancheng Cai et al. (2021) carried out the numerical assessment and web-crippling behaviour of stainless steel subjected to elevated temperatures. The results showed that new design equations and DSM analysis were developed for IOF, ITF, and IL loading conditions under high temperature effects [25]. Hai-Ting Li et al. (2022) proposed a new DSM approach for web-crippling design of high strength steel square and rectangular hollow sections at elevated temperatures, including CFS stainless hollow sections under ambient conditions [26].

### *Research Significance*

High-performance CFS members are expected to satisfy the strength, durability, and cost effectiveness for its intended usage. From a detailed literature survey, it is understood that experiments and numerical models on web-crippling behaviour of CFS elements under different load conditions are extensively studied. Flexural and shear resistance of high-performance CFS members were explored by researchers. Fire and corrosion are the essential durability related properties yet to be analysed for high performance CFS members. However, web-crippling behaviour of high-performance CFS under prolonged temperatures is scarce in the literature and very few researchers have paid attention to numerical studies on web-crippling behaviour of high-performance CFS sections at high temperatures. It is the primary research gap identified, and will be highly useful for the design applications by structural engineers to understand the importance of high-performance CFS when subjected to fire accidents. The following were the objectives of this study:

- To study the post-fire performance and web-crippling behaviour of high-performance CFS elements subjected to elevated temperature as per ISO 834 standard fire curve.
- Influence of web holes on web-crippling strength of high-performance CFS sections exposed to elevated temperature under ITF and ETF load cases.
- Investigations are conducted to examine the load-deflection behaviour, web-crippling strength, and failure modes of the CFS specimens heated and cooled by different mode.
- To understand the web-crippling response of high-performance CFS specimens, a FEM model was developed and validated with test results.

## **2. Experimental Investigation**

### *2.1. Overview*

In this study, high-strength steel grade of E350 was considered. This is the section widely used in the Industrial buildings as purlin and available in the market. This section is cost effective and suitable for satisfying bending capacity. All the specimens were exposed to elevated temperatures at different durations of heating, namely 30 min, 60 min, 90 min, and 120 min following ISO834 curve. The mechanical properties of all the coupon specimens shown in Table 1, including reference (at room temperature), were determined by performing tensile tests on specimens. Also, one of the objectives of this research work was to identify the performance of specimens at different cooling conditions (air-cooled and water-cooled). After the fire accidents, the structural members may be cooled by water as a forced cooling method. After the severe exposure to fire, the residual mechanical properties of the section may vary, and it is based on exposure duration and cooling. In the absence of water cooling, the members experience gradual and natural air-cooling process. Therefore,

two types of cooling were considered in the proposed study. Similar studies were carried out by Jie Lu et al. [27] and Chong Ren et al. [28], considering different cooling conditions.

**Table 1.** Mechanical properties of unheated and heated high-performance E350 CFS.

Duration of Heating (min)	Yield Strength-AC (MPa)	Yield Strength-WC (MPa)	Ultimate Strength-AC (MPa)	Ultimate Strength-WC (MPa)	Elastic Modulus-AC (GPa)	Elastic Modulus-WC (GPa)	% Elongation-AC	% Elongation-WC
Reference	415	NA	544	NA	211	NA	0.43	NA
30	335	318	425	401	157	150	0.38	0.36
60	255	237	385	360	146	142	0.35	0.33
90	183	165	250	202	102	92	0.3	0.24
120	147	140	210	190	65	54	0.21	0.20

AC—Air cooled, WC—Water cooled, NA—Not Applicable.

## 2.2. Specimen Details

High-performance CFS C-section with lips, which are readily available in industry, were selected based on the required dimensions. The steel channels were formed using a press-brake cold-rolling process to achieve the desired shape and dimension. The dimensions of the section were chosen with a web depth of 200 mm, flange width of 60 mm, and a lip depth of 20 mm for the study. The thickness of the section was 2 mm. The length of specimens varied based on end conditions selected.

For the ITF condition, the specimen length had to be greater than 1.5 h from the edge of the bearing to the end of the member as specified in AISI S909-13 [29]. Similarly, for the ETF condition, the length of the specimen had to be equal to or less than 1.5 h from the bearing edge to the end of member as shown in Figure 2. Two types of specimens were considered such as CFS beam without circular hole (WH) and with a circular hole (WCH) in an unfastened condition. The aspect ratio ( $a/h$ ) for the web perforation was taken as 0.5, which is calculated by flat web depth ( $h$ ) of the section deducting the corner radius, which is approximately 1.5 times the thickness of the section. The web perforation was made exactly beneath the mid-depth of the web portion using a computer numerically controlled (CNC) wire-cutting machine.

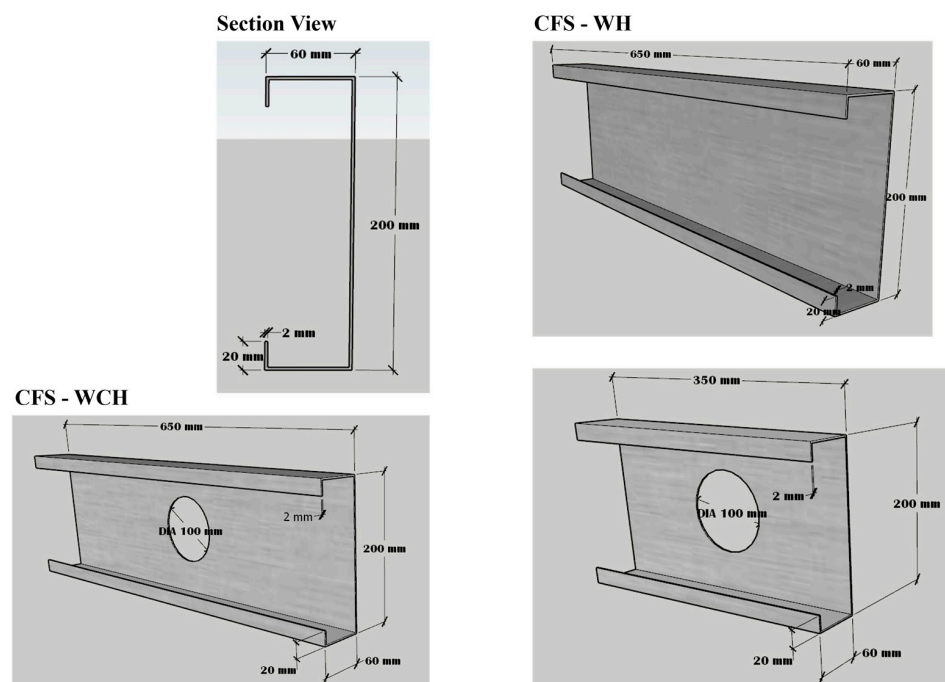


**Figure 2.** Section geometry of two different CFS sections with and without hole.

### 2.3. Elevated Temperature Test on CFS Sections (Heating and Cooling)

In the study, a digital controlled electrical coil furnace with the dimensions of  $700 \times 400 \times 400$  mm was used to heat the CFS specimens. The heating procedure for the CFS specimens was followed as per the ISO 834 standard fire curve [30]. A total of 52 CFS specimens were heated, with four different heating durations such as 30 min (821 °C), 60 min (925 °C), 90 min (986 °C), and 120 min (1029 °C). The CFS specimens were placed in the furnace in such a way that equal temperature distribution ensured on the entire specimen, as shown in Figure 3a.

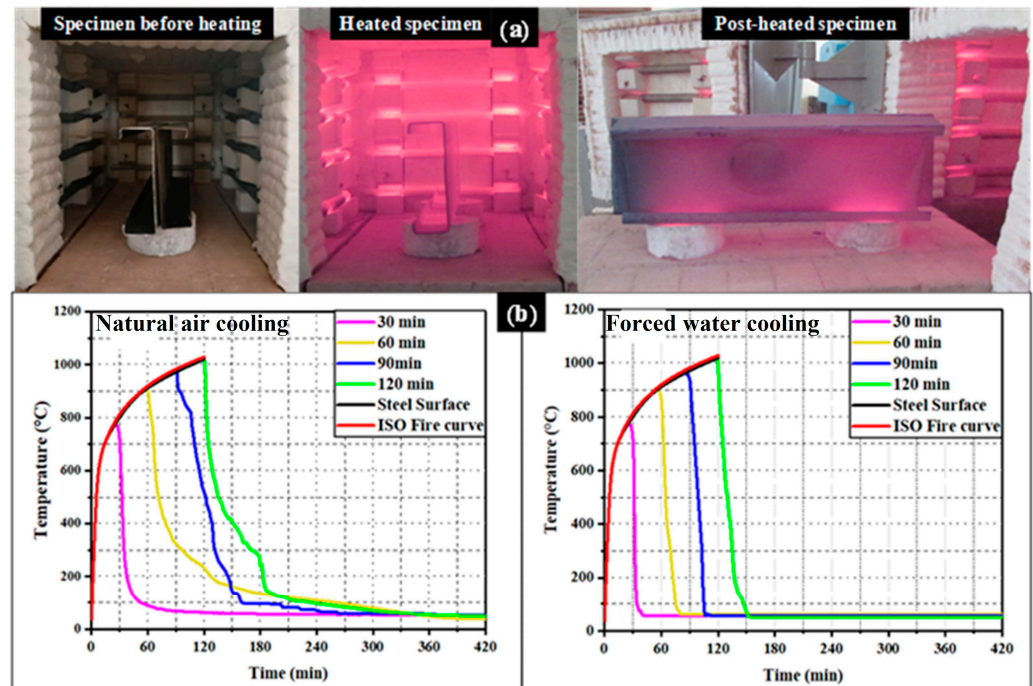


**Figure 3.** View of (a) CFS specimen under elevated temperature. (b) Heating–cooling regime of CFS specimen.

During the heat exposure, the temperature values of the coil (T1) and surface temperature of CFS (T2) were recorded using K-type thermocouples, which were connected to a micro panel unit for the storage of temperature values. When the furnace reached to target temperature, it switched off automatically, and the coil temperature started to decline towards ambient conditions. During this stage, two types of cooling conditions were adopted to cool the CFS specimens, namely natural air cooling and forced water cooling, and the temperature values were noted using an infrared thermometer. The recorded heating cooling regime is shown in Figure 3b.

Based on the recorded time temperature values, it was observed that the applied temperature and surface temperature of the CFS sections were nearly the same. During the process of cooling, the air-cooled specimens took some time to gradually decrease to the ambient temperature. However, in the water-cooled case, the temperature decreased rapidly, to attain the ambient temperature.

### 2.4. Material Properties

The mechanical properties of CFS sections were determined through tensile coupon testing. The C-sections were heated following the ISO 834 fire curve for various heating durations and cooled by air- and water-cooling conditions. Coupon specimens were extracted from the web and flange portions along the length of the member using a CNC wire-cutting machine, and the specimen details are depicted in Figure 4a. This is based on geometric imperfection of the section and a greater number of specimens can be extracted along the length when compared to depth. The dimensions of the steel coupon

were chosen according to the specifications in ASTM E8/E8 [31]. A universal tensile testing machine with a 50 kN ultimate load capacity was used in the study, and a loading rate of 0.5 mm/min was maintained throughout the test for all the specimens until failure, as shown in Figure 4b. The stress–strain behaviour of the steel coupon specimens was recorded using a microprocessor-based strain gauge attached to the mid-portion of the specimen. The strain gauge sensor, having 60 mm length and 120  $\Omega$  resistance with a 1000 micro strain capacity was connected by the quarter-bridge circuit connection method. The mechanical properties, such as yield strength (at 0.2% proof stress), ultimate strength, and modulus of elasticity, were determined from the stress–strain response shown in Figure 5 and are presented in Table 1.

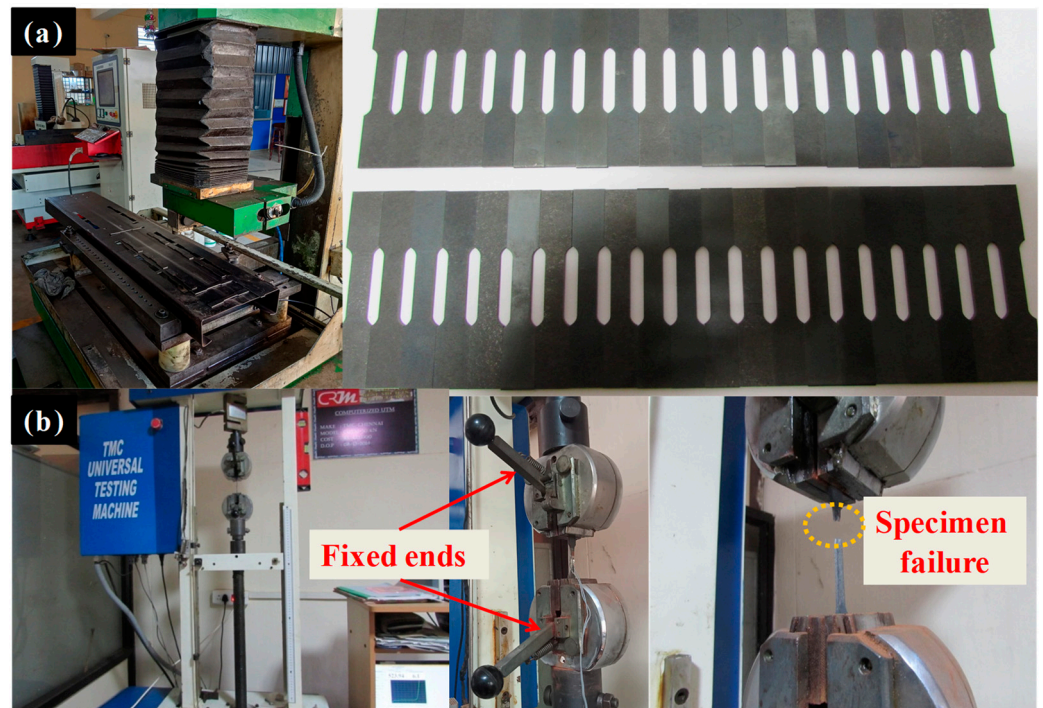


Figure 4. View of tensile test program (a) extracting of coupon specimens from CFS section (b) failure of coupon specimen.

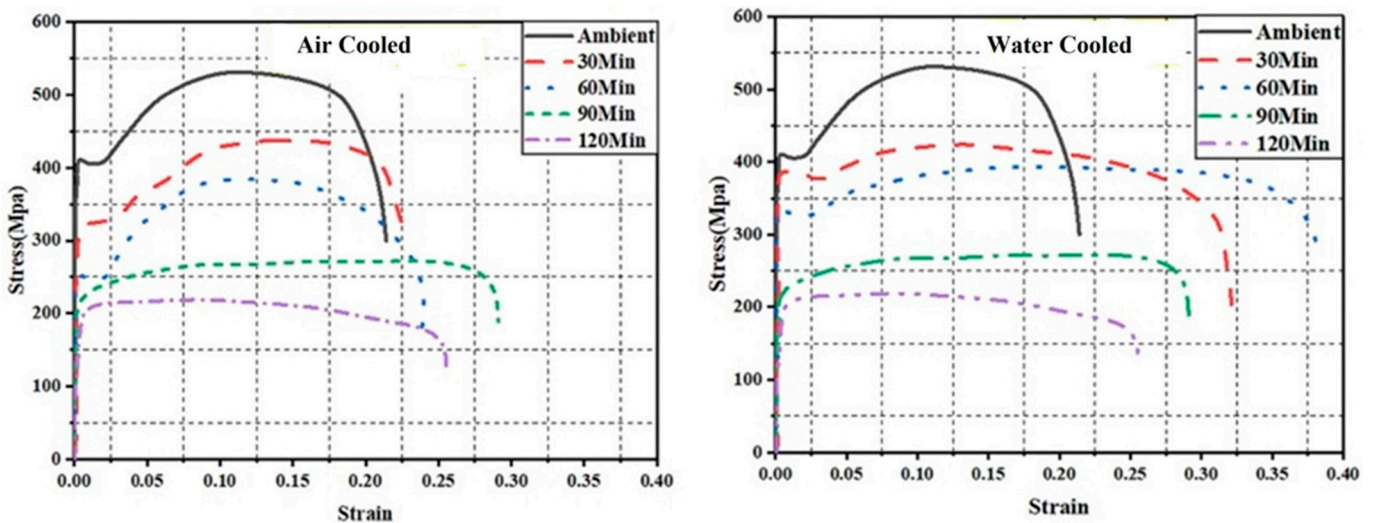
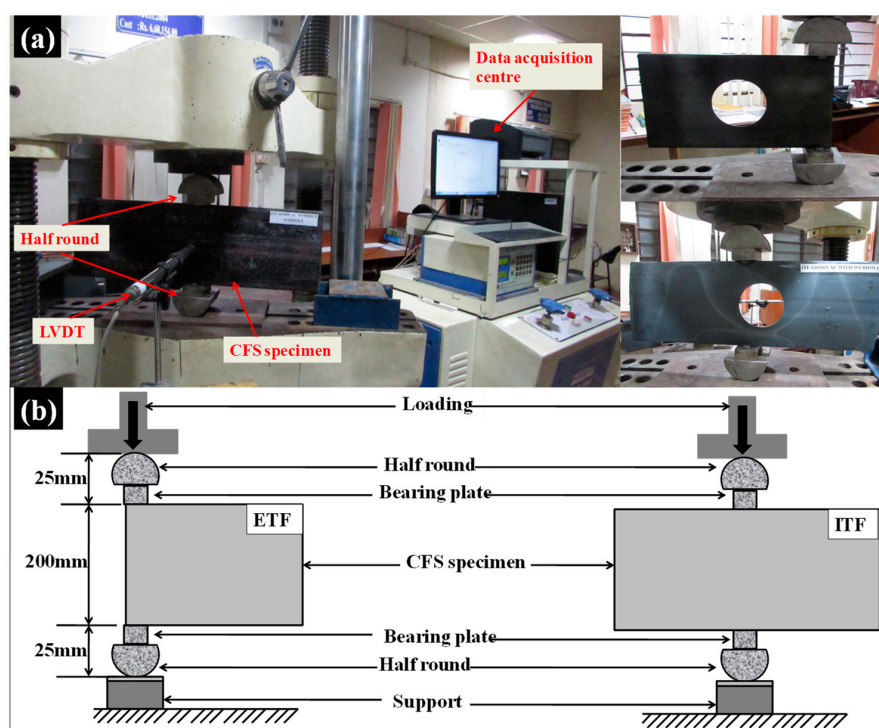


Figure 5. Stress vs. strain for air-cooled and water-cooled specimens.

### 2.5. Experimental Setup

A test was carried out to evaluate the web-crippling capacity of high-performance CFS sections made of carbon steel. A total of 52 CFS specimens were tested under ITF and ETF load conditions, as shown in Figure 6a, and a schematic diagram is represented in Figure 6b. Two equal-sized steel bearing plates having length 50 mm were used to apply concentrated loads on the top and bottom flanges of the section. Two half-rounds were fixed in the bearing plates, which typically act as a pin support conditions to transfer the vertical load onto the specimen. A computerized Universal Testing Machine (UTM) with a maximum load carrying capacity of 1000 kN was used in the study, the UTM with a load rating of 10 N/mm/s was used. An LVDT was located in the web portion of the section used to record the corresponding displacement values with respect to the applied load. All CFS specimens were tested until failure, the load–displacement response and failure modes were noted and presented in the results.



**Figure 6.** View of CFS specimen under ETF and ITF load conditions: (a) experimental, (b) schematic test setup.

## 3. Results and Discussion

### 3.1. Load-Deflection Behaviour of CFS Beams

Experiments were conducted to evaluate the load-deflection behaviour of the high performance CFS specimens subjected to standard fire temperature. Figures 7 and 8 shows the load-deflection behaviour of the exposed CFS-WH, and CFS-WCH beams under ETF and ITF load cases. The experimental results are discussed extensively, focusing on the influence of temperature, cooling methods, effect of web hole, and loading conditions of CFS specimens.

#### 3.1.1. Load-Deflection Behaviour at ETF Condition

For all the reference specimens, the load initially increased linearly with minimum deformation. After reaching the ultimate load, the deflection started to increase with a variation in yielding. However, with increasing temperature, particularly after 60 min, a decrease in strength and an increase in deformation were observed for both the WH, and WCH specimens.

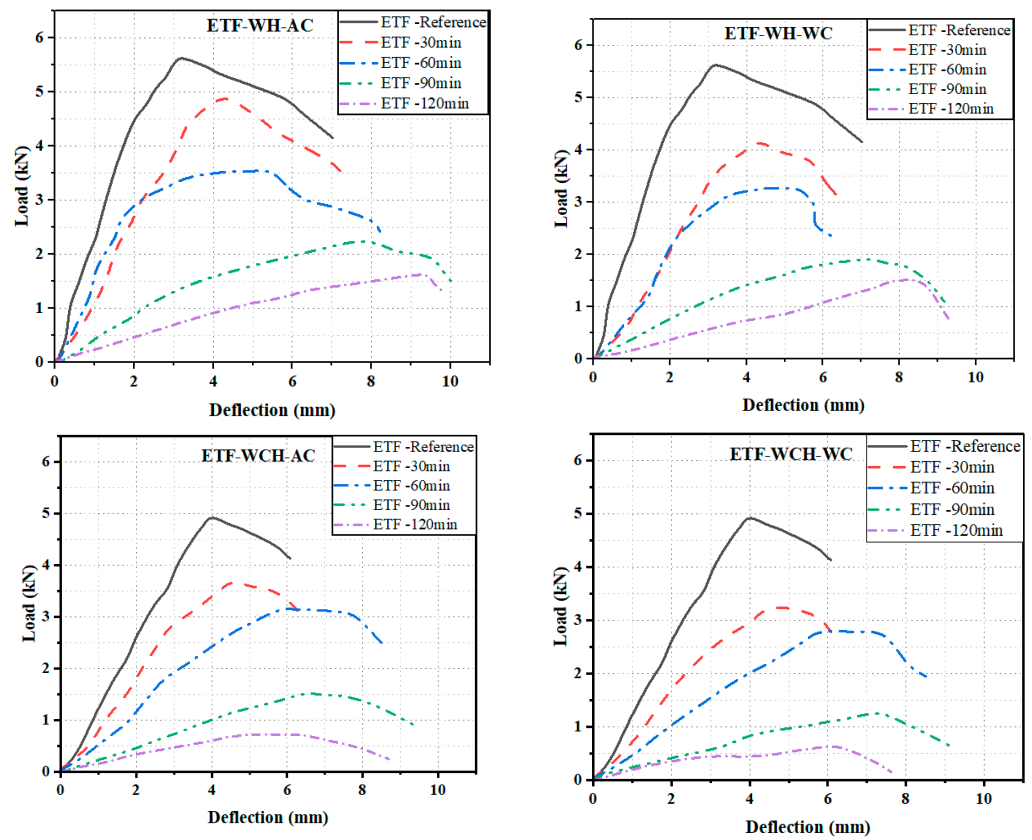


Figure 7. Load-carrying capacity and deflection behaviour of high performance CFS sections under ETF load case.

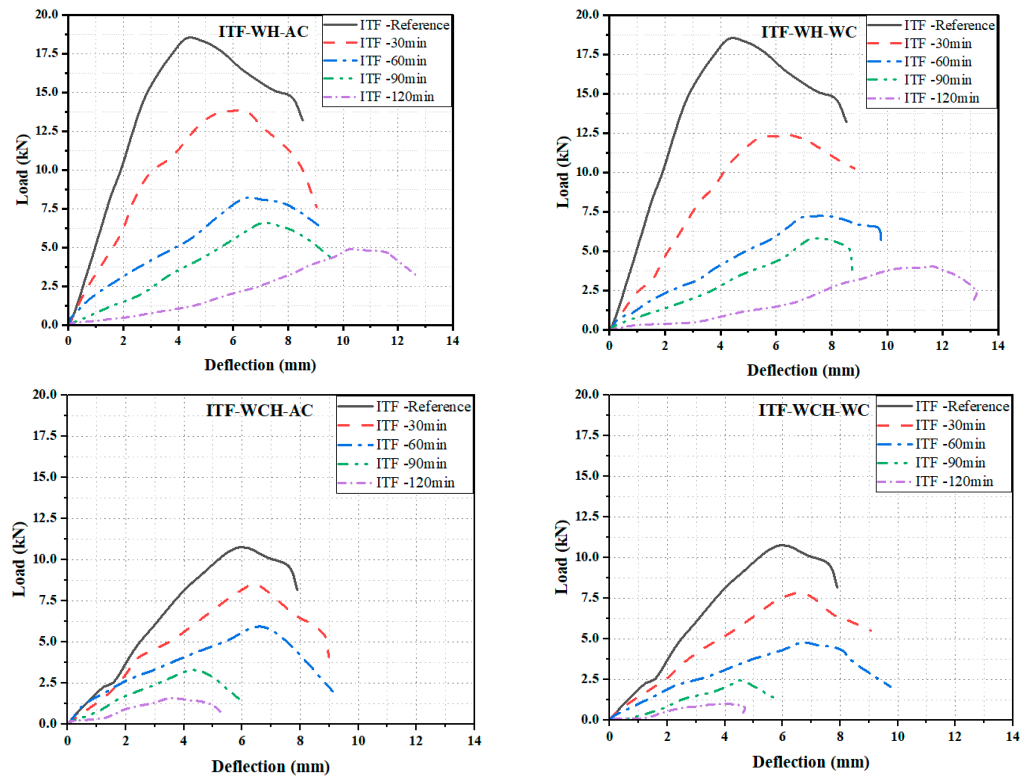


Figure 8. Load-carrying capacity and deflection behaviour of high performance CFS sections under ITF load case.

From the load-deflection behaviour shown in Figure 7, the plotted results demonstrate that the reference (unheated) WH, WCH specimens exhibited a web-load-carrying capacity of 5.61 kN and 4.91 kN, respectively. At exposure of 30–60 min, the web-load-carrying capacity of WH specimens decreased to 4.86 kN and 3.52 kN, while for the WCH specimens, it decreased to 3.65 kN and 3.13 kN. Further increasing the temperature exposure to 90–120 min, the web-load-carrying capacity of the WH and WCH specimens showed a drastic reduction in strength to 2.21 kN, 1.60 kN and 1.5 kN, 0.71 kN, respectively. Similarly, all the water-cooled specimens showed a moderate strength loss of about 7.5–10% compared to the air-cooled specimens for WH. However, in the case of WCH, the strength loss was slightly higher in the range of 7.5–15% compared to WH. After being exposed to elevated temperatures 60 and 120 min, the residual strength decreased to 37.20% to 71.44% for WH and 36.27% to 85.38% for WCH. Hence, these observations indicate that the decrease in web-carrying capacity of CFS beams is mainly attributed to the critical temperature and prolonged heating duration. Also, web perforation ratio plays a significant role in load carrying capacity of sections exposed to elevated temperatures. When the web perforation ratio increases, the web-crippling capacity of section decreases and fails quickly under higher durations of heating. Consequently, the steel beams experience a loss of rigidity, degradation of stiffness, and strength properties [2].

From the results of web deformation behaviour of CFS beams, it was observed that the reference specimens exhibited high web-load-carrying capacity with lower deformation values. At the elevated temperatures (30–120 min), the lateral deformation values for WH specimens ranged between 4.23 mm and 9.05 mm, while for WCH specimens, they ranged between 4.52 mm and 6.45 mm. In the case of water-cooled specimens, an increase in temperature exposure also resulted in increased deformation values and this increase was approximately 2.5–3.75 mm compared to the air-cooled specimens.

### 3.1.2. Load-Deflection Behaviour at ITF Condition

The load-deflection graph indicates that the exposed CFS specimens exhibited a significant loss of strength as the deflection value increased. The loss in strength can be attributed to the degradation of rigidity, stiffness, and strength properties of CFS beams, resulting in lower strength carrying capacity and higher deformations [20].

Figure 8 illustrates the load-deflection behaviour of a CFS specimen under ITF conditions. The maximum web-load-carrying capacities of the CFS beams were observed for the reference specimens (WH and WCH), measuring 18.48 kN and 10.72 kN, respectively. Notably, the ITF specimen exhibited approximately a 10–15% higher carrying capacity compared to the ETF condition. Similar trends were observed in the previous studies [1,2,23]. At elevated temperatures, the CFS WH and WCH specimens displayed a reduction in web-load-carrying capacities, measuring 13.82 kN, 8.14 kN, 6.58 kN, 4.86 kN and 8.5 kN, 5.8 kN, 3.27 kN, 1.56 kN, for 30, 60, 90, and 120 min, respectively. Furthermore, the web strength reduction in CFS specimens was more pronounced in the water cooling compared to air cooling. The cooling of steel specimens with water results in reduced yield strength and ductility due to changes in the microstructure [1]. Therefore, the residual moment carrying capacity of the steel primarily depends on the temperature magnitude, heating duration, and cooling method. Interestingly, the better performance was observed in the results of ITF reference compared to ETF.

From Figure 8, it can be observed that the deflection values of CFS increased with longer durations of fire exposure. For temperature exposure below 60 min (925 °C), the deflection values were roughly equal to those of the unheated CFS specimen (reference). At higher temperatures (30–120 min), the lateral deflection values for WH specimens were 6.05 mm, 6.38 mm, 7.09 mm, and 10.19 mm, while WCH specimens displayed the deflection values of 6.41 mm, 6.33 mm, 4.42 mm, and 3.53 mm. In the case of water-cooling specimens, it was observed that the deflection values increased by approximately 3.5–4.25 mm compared to air cooling specimens.

Similarly for ITF condition, at higher durations of heating, the effect of increased web perforation became more pronounced. Elevated temperatures can cause the material properties of steel, such as strength and stiffness, to degrade. As a result, the weakened web with higher perforation ratio was more susceptible to buckling or collapsing under compressive loads when exposed to elevated temperatures for longer periods.

### 3.2. Failure Modes of High Performance CFS Specimens

All the CFS specimens were tested until its failure and failure modes were noted. The failure behaviour of the specimen mainly depends on duration of heating, magnitude of temperature, and cooling type. Web crippling was observed as one of the failure modes during the testing process. The web-crippling failure mode of CFS specimens under ETF and ITF is illustrated in Figure 9. The failure pattern and modes of the specimen for heating and cooling are discussed below.

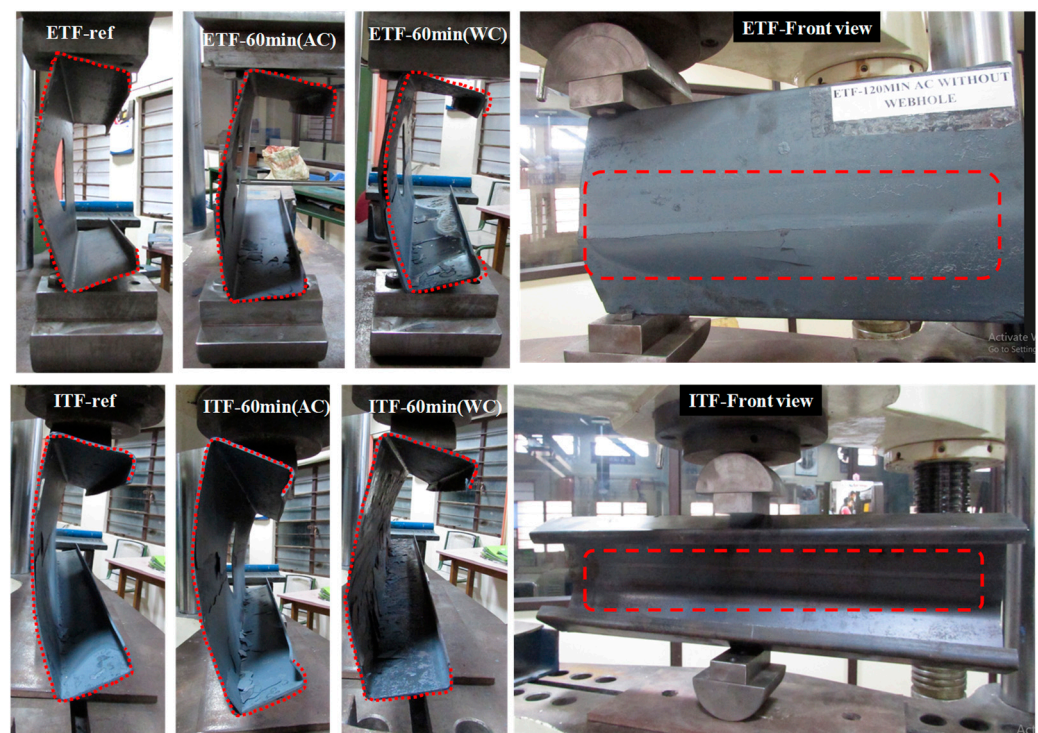


**Figure 9.** View of web-crippling failure of CFS specimens under ETF and ITF load cases.

The reference CFS beams (unheated) also exhibited web crippling under both ETF and ITF loading conditions. Initially, the web section of the specimen began to yield. However, at around 75% to 80% of the applied load, web crippling suddenly occurred, resulting in compression deformations of the top and bottom flanges. At elevated temperatures of 30, 60, 90, and 120 min, the web-crippling failure modes were observed. However, the stages of failure varied. For exposure durations of 30 and 60 min, the specimens initially exhibited yielding behaviour, followed by web-crippling failure at around 50% to 60% of the applied load. In contrast, at higher temperatures of 90 and 120 min, yielding behaviour was not observed, and the specimens failed directly without any indication, experiencing sudden web-crippling failure. Similar failure modes and behaviour were also observed in the water-cooled specimens.

The water-cooled CFS specimens exhibited an earlier failure compared to the air-cooled specimens, which can be attributed to the weakening of the water-cooled section. This weakening is evident from the results of ultimate load and deflection. The primary cause of this observed behaviour is due to its higher reduction in yield strength, ultimate strength, and elastic modulus of the water-cooled CFS sections.

During the process of water cooling, the material undergoes a sudden transformation in phase due to the thermal-shock-induced stress. This transformation leads to surface cracks and deterioration in bond strength between carbon atoms on the steel surface. Although the water-cooled specimens demonstrate ductility under ETF and ITF loading, their reduction in material strength and stiffness resulted in sudden failure [22].

The failure behaviour of the specimens is dependent on the influence of heating and cooling, which plays a vital role. The specimens exhibit reduced strength as the temperature varies with different heating durations. Under both ETF- and ITF-loading conditions, the specimens experienced significant lateral web deformations compared to the unheated specimens.

## 4. Finite Element Modelling

### 4.1. Numerical Simulation

The present study aimed to develop a numerical modelling on web-crippling behaviour of carbon CFS C sections under elevated temperature using ABAQUS software (version 6.13) [32]. Four types of FEM models were developed in the study, including CFS-WH- and CFS-WCH-lipped C sections under ITF and ETF conditions exposed to high temperatures. The main aim of the study was to simulate the web-crippling experimental setup, validate with the experimental results and failure behaviour of CFS sections, which are presented in Section 4.5.

### 4.2. Modelling and Material Property

In this section, the CFS specimens were modelled with exact dimensions, which were used in the experiments. The CFS specimens were modelled based on the dimensions given in Figure 2. Material property of the CFS specimens is the important factor to validate the accuracy of results and failure behaviour [2]. Tensile coupon specimens were made and tested under ambient and elevated temperature conditions. Material properties used for developing the web-crippling model of CFS beam are shown in Table 1. The material properties such as yield strength, ultimate strength, elastic modulus, strain and Poisson's ratio values were consigned in the respected model. The non-linear engineering (stress-strain) properties were converted into true material properties in the FE modelling, and the equations are presented below.

$$\sigma_{\text{true}} = \sigma (1 + \epsilon) \quad (1)$$

$$\epsilon_{\text{true(pl)}} = \ln(1 + \epsilon) - \frac{\sigma_{\text{true}}}{E} \quad (2)$$

where  $\sigma_{\text{true}}$  is true stress,  $\sigma$  and  $\epsilon$  are engineering stress and strain in the ABAQUS [2].

### 4.3. Element Type and Meshing

The CFS channel sections were modelled with S4 shell elements, which is suitable to analyse the behaviour of thin members. The S4R element is a 4-noded quadrilateral stress/displacement shell element with reduced integration and hourglass control, utilized a first order interpolation function. The load plate and support-bearing plate were modelled using rigid (R3D4) elements. Similar element types were adopted for developing numerical models on web crippling under different load conditions by researchers in the past studies [3,5–7].

The mesh size of element is one of the essential parameters for performing the FE analysis, because it specifies the computational time and level of exactness in the results. Due to this, a mesh sensitive analysis was carried out in the study to prefer the suitable mesh size for CFS C sections under ITF and ETF load condition, which is presented in Figure 10. Similar results were reported in previous web-crippling studies [3,4].

Therefore,  $5 \times 5$  mm mesh size was used in the web and flange regions of the model and  $1 \times 5$  mm mesh size was used in the corner regions of the CFS C section. For modelling, the web holes in the specimens, mesh size of  $5 \times 5$  mm, was used. The load and support-

bearing plate (discrete rigid element) were not directly associated with the web-crippling load-carrying capacity. For that reason,  $10 \times 10$  mm mesh size was assigned for the rigid elements, as it does not affect the FE analysis and its accuracy. CFS C sections modelled with and without hole are shown in Figure 11.

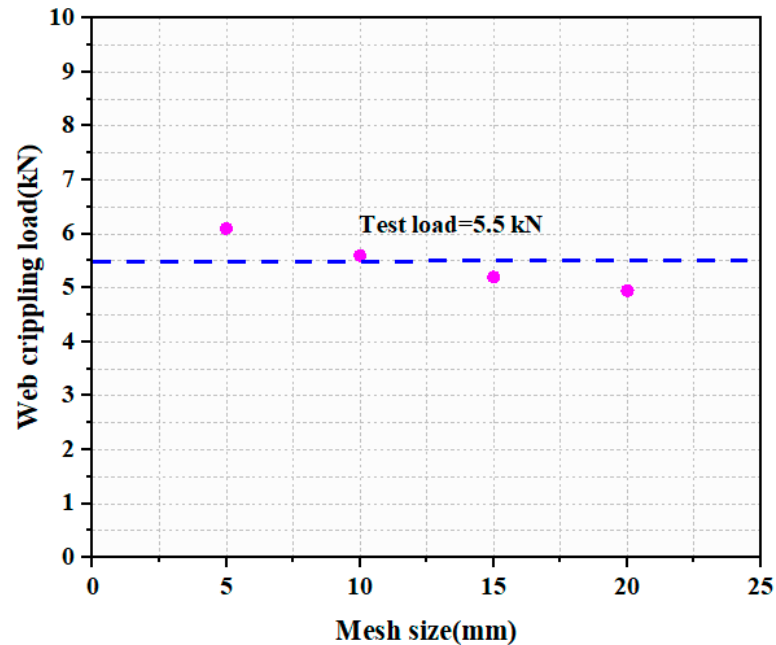


Figure 10. Mesh-sensitive analysis.

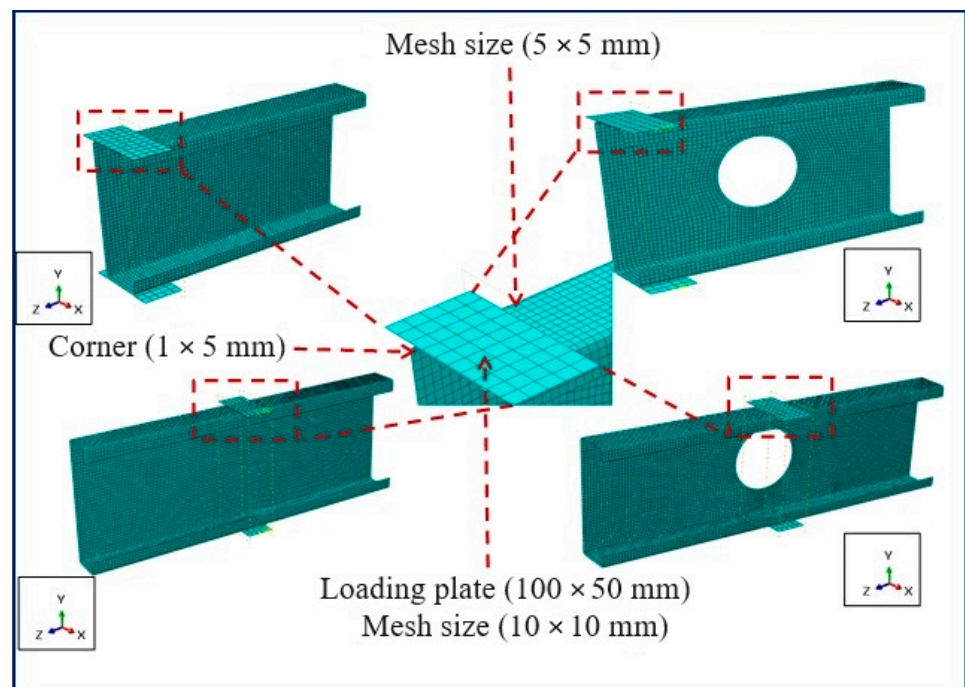


Figure 11. Meshing of CFS specimens in FE model.

#### 4.4. Contact Properties, Loading and Boundary Conditions

To simulate the boundary and loading conditions in CFS section, two reference points were created in the load and support bearing plate (RP1 and RP2). In the FE model, to make contact between the CFS specimen surfaces, the bearing plate surface was modelled using contact pair interaction type in ABAQUS. Based on previous studies [2,3,5,8],

surface–surface contact property was assigned in between the sections. The rigid plates were selected as the master surface, flat flange, and corner radius portions of the beam as the slave surfaces to simulate the proper interaction properties. Therefore, to ensure the gap between rigid element and CFS section, a “face-to-face” position constraint was used, which restrained the overlaps of two contact surfaces. The interaction property was defined as a normal and tangential behaviour and it was assigned between the CFS specimen and bearing plates. Therefore, hard contact is preferred and plenty friction coefficient of 0.4 was assigned to represent the friction-slip behaviour during the FE analysis.

Figure 12 shows the featured boundary conditions of CFS specimen under web-crippling condition. To generate the loading effect as experiment setup, translation movements were considered in  $U_x$  and  $U_y$  directions along with all the rotational movement,  $UR_3$  direction was also restrained at the top bearing plate (loading point). The vertical displacement of 20 mm was applied in top bearing plate through the ( $U_y$ ) direction. The applied displacement load was controlled by using ABAQUS’s smooth step amplitude function (amp1) to produce a slower initial stage displacement and to develop smooth deformation in the structure. All the translation and rotational movements, except rotation movement in  $x$  and  $y$  directions, were also restrained in the bottom bearing plate.

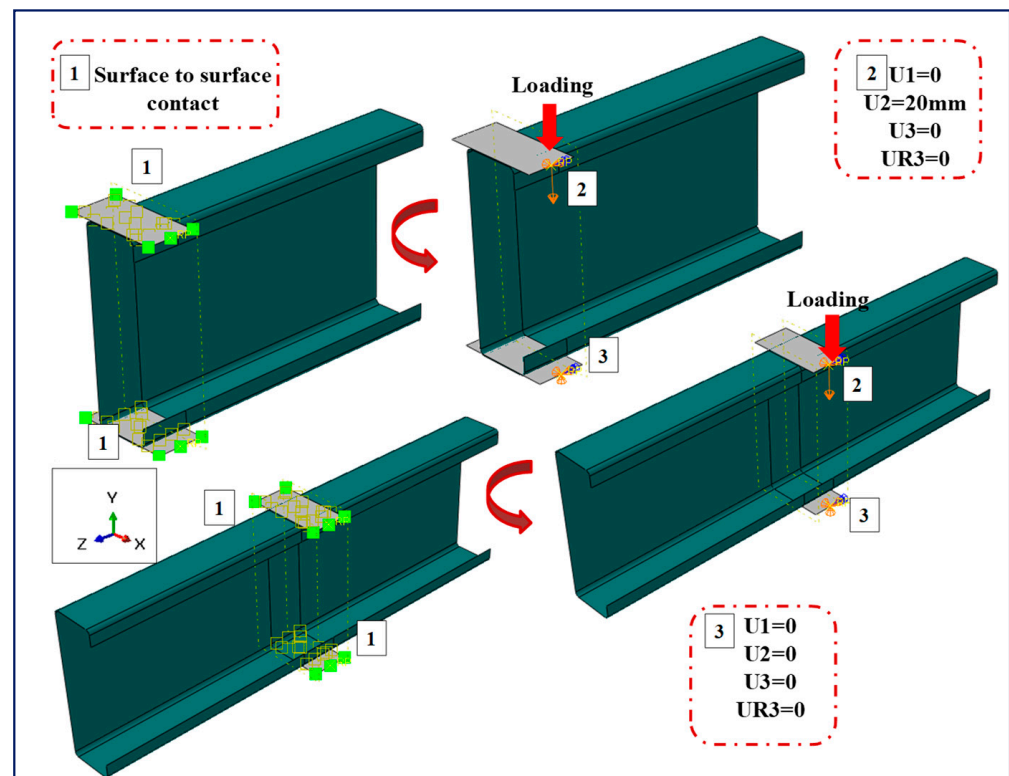


**Figure 12.** Contact properties and boundary conditions in FE model.

#### 4.5. Geometrical Imperfections

Previous studies stated that the web-crippling load-carrying capacity was not considered the global imperfections [3,5]. From recent studies, it was found that geometric imperfections of web-crippling under load conditions was less than 2–3%, respectively [5,6]. Therefore, the geometrical imperfection in the FE model of the CFS channel section under ITF and ETF conditions is neglected.

#### 4.6. Validation

The results obtained from the numerical analysis of FE models are compared with the experimental test results, which were explained in Sections 4.6.1 and 4.6.2.

#### 4.6.1. Comparison of Load-Deflection Behaviour (Experimental Results vs. FEM)

This study aimed to compare the FE model's ultimate web-crippling capacity and failure modes with experimental results of CFS C channel sections. It can be observed from the results that the test results closely matched with the numerical results.

The web-crippling capacity of CFS sections obtained from experiments and FEM are shown in Table 2 and seems to be conservative. Figures 13 and 14 shows the comparison of web-crippling load deflection behaviour obtained from the experimental investigation with FEM. It is interesting to highlight that, considering all the FE models, the percentage error was calculated and was found between 5 and 10%, as compared with experimental results.

**Table 2.** Web-crippling capacity of section (Experimental vs. FEM)—ETF and ITF condition.

S. No	Duration of Heating and Cooling Type	Temperature as per ISO 834	Web-Crippling Capacity (kN)							
			ETF WH		ETF WCH		ITF WH		ITF WCH	
			Exp	FEM	Exp	FEM	Exp	FEM	Exp	FEM
1	Reference	0 °C	5.619	5.737	4.914	5.292	18.565	19.103	10.795	11.376
2	60 min AC	925 °C	3.529	3.692	3.131	3.385	8.281	8.640	5.963	6.361
3	60 min WC	925 °C	3.263	3.573	2.782	2.986	7.238	7.503	4.752	4.962
4	120 min AC	1029 °C	1.605	1.780	0.718	0.768	4.933	5.232	1.621	1.023
5	120 min WC	1029 °C	1.490	1.585	0.624	0.644	4.047	4.195	1.743	1.083

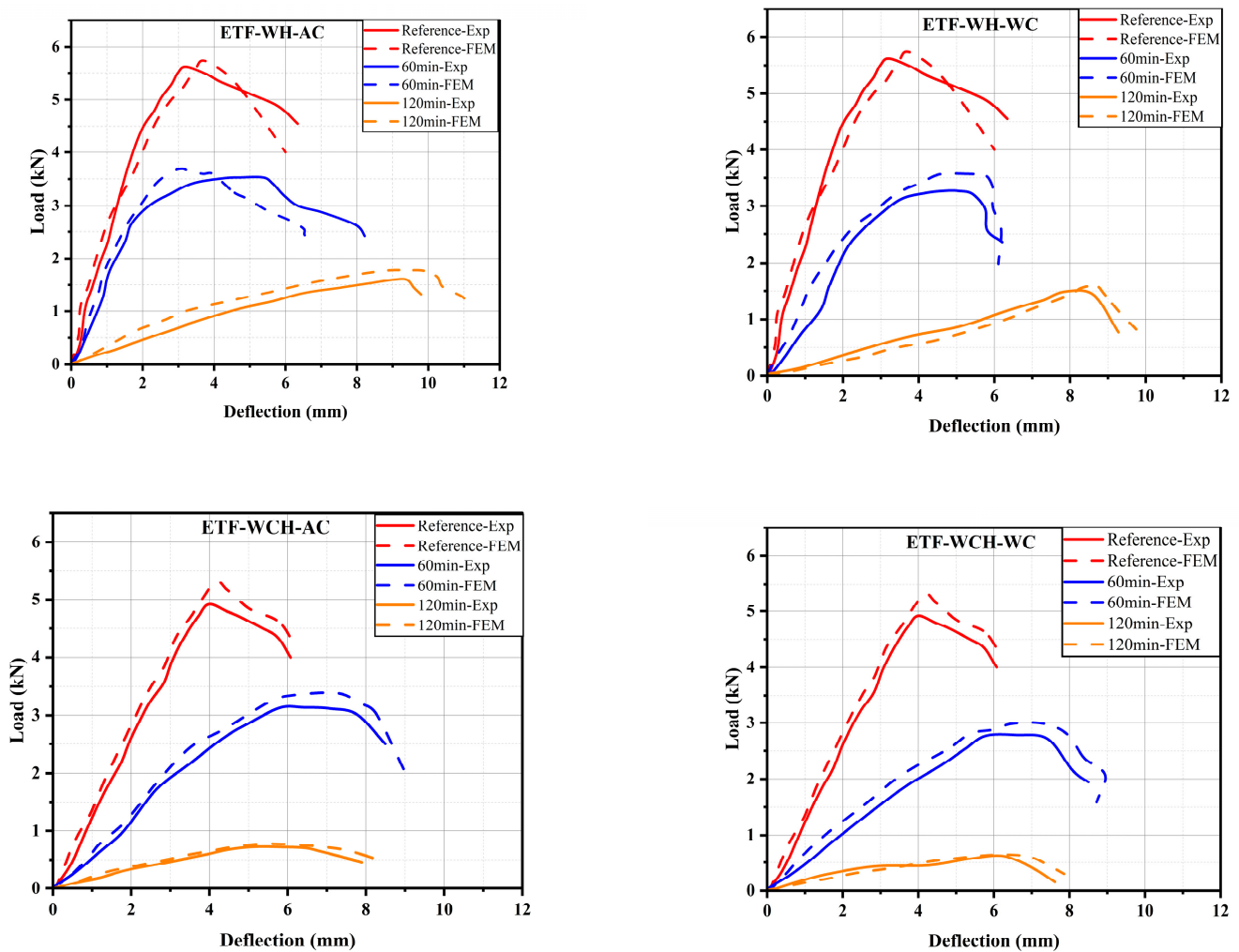


**Figure 13.** Comparison between load-deflection behaviour of experiment and FEM of ETF specimens (WH and WCH).

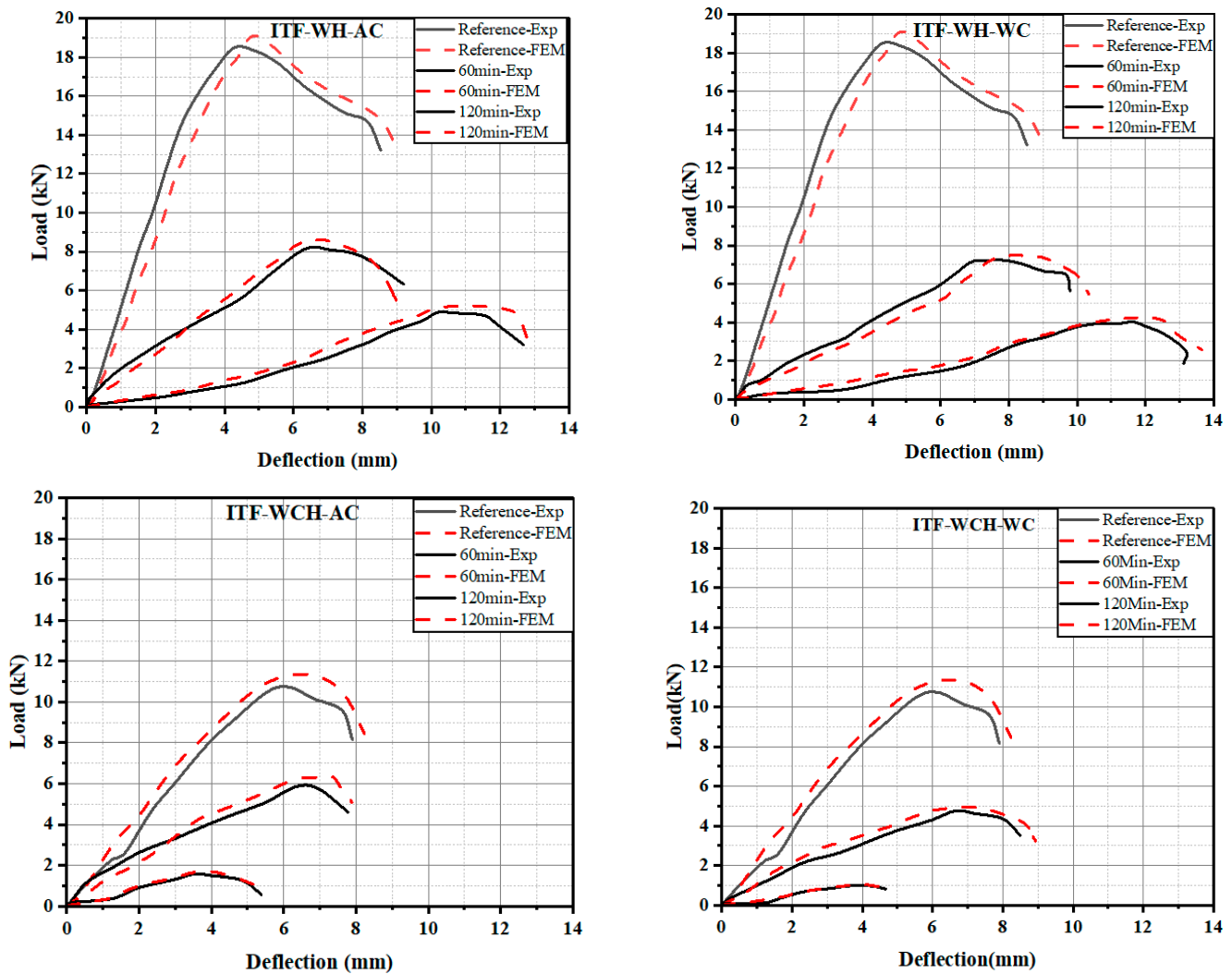


**Figure 14.** Comparison between load-deflection behaviour of experiment and FEM of ITF specimens (WH and WCH).

#### 4.6.2. Failure Modes (Experimental Results vs. FEM)

Tables 3 and 4 depicts the web-crippling behaviour of experimental and FEM model of CFS subjected to elevated temperature under both cooling conditions and different load case. The failure modes of the CFS C channel sections at ambient, air-cooled (30, 60, 90, and 120 min) heated, and water-cooled (30, 60, 90, and 120 min) heated conditions were compared between experimental and FEA. The obtained failure modes were similar to that of FEA simulation results. Web-crippling failure was observed for specimens at ambient and elevated temperature (air and cooling conditions). Therefore, the proposed FE model can predict the accurate web-crippling capacity of any other cold-formed steel sections, considering the effect of elevated temperature and cooling conditions, respectively.

Web yielding occurred in both ETF and ITF conditions. Web-crippling failure was observed within the web portion of the specimen. It was due to the exposure of higher durations of heating, i.e., at 60 min and 120 min, the physical appearance of sections varied, i.e., colour change was visualized and peeling was noticed in the specimens. There was no evidence of crushing of flanges in both ETF and ITF conditions.

**Table 3.** View of failure mode images under ETF loads (Experiment vs. FEM).

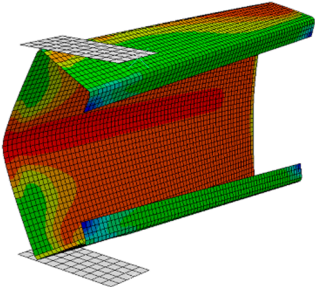
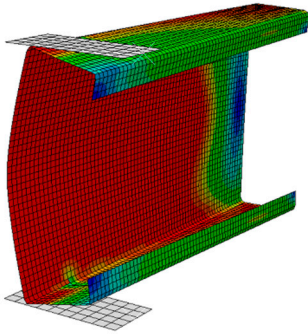
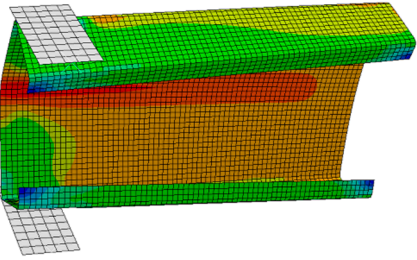
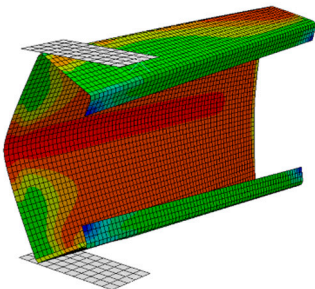
Duration of Heating	Exp	Air Cooled-ETF-without Hole	FEM
Reference		<p>S, Mises SNEG, (fraction = -1.0) (Avg: 75%)</p> <ul style="list-style-type: none"> <li>+3.387e+02</li> <li>+3.128e+02</li> <li>+2.870e+02</li> <li>+2.612e+02</li> <li>+2.354e+02</li> <li>+2.095e+02</li> <li>+1.837e+02</li> <li>+1.579e+02</li> <li>+1.321e+02</li> <li>+1.062e+02</li> <li>+8.042e+01</li> <li>+5.460e+01</li> <li>+2.877e+01</li> </ul>	
60 min		<p>S, Mises SNEG, (fraction = -1.0) (Avg: 75%)</p> <ul style="list-style-type: none"> <li>+1.642e+02</li> <li>+1.514e+02</li> <li>+1.386e+02</li> <li>+1.258e+02</li> <li>+1.130e+02</li> <li>+1.002e+02</li> <li>+8.737e+01</li> <li>+7.457e+01</li> <li>+6.176e+01</li> <li>+4.896e+01</li> <li>+3.615e+01</li> <li>+2.335e+01</li> <li>+1.054e+01</li> </ul>	
120 min		<p>S, Mises SNEG, (fraction = -1.0) (Avg: 75%)</p> <ul style="list-style-type: none"> <li>+9.305e+01</li> <li>+8.595e+01</li> <li>+7.884e+01</li> <li>+7.173e+01</li> <li>+6.461e+01</li> <li>+5.750e+01</li> <li>+5.039e+01</li> <li>+4.328e+01</li> <li>+3.617e+01</li> <li>+2.906e+01</li> <li>+2.194e+01</li> <li>+1.483e+01</li> <li>+7.720e+00</li> </ul>	
Duration of Heating	Exp	Water Cooled-ETF-without Hole	FEM
Reference		<p>S, Mises SNEG, (fraction = -1.0) (Avg: 75%)</p> <ul style="list-style-type: none"> <li>+3.387e+02</li> <li>+3.128e+02</li> <li>+2.870e+02</li> <li>+2.612e+02</li> <li>+2.354e+02</li> <li>+2.095e+02</li> <li>+1.837e+02</li> <li>+1.579e+02</li> <li>+1.321e+02</li> <li>+1.062e+02</li> <li>+8.042e+01</li> <li>+5.460e+01</li> <li>+2.877e+01</li> </ul>	

Table 3. Cont.

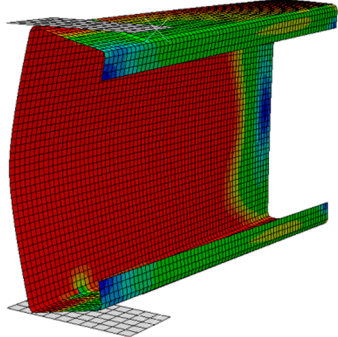
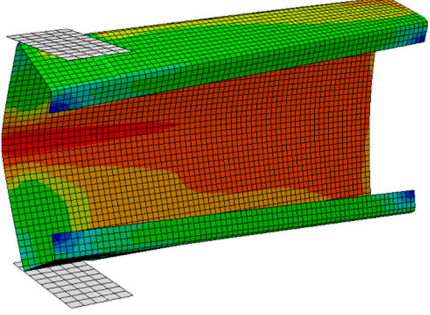
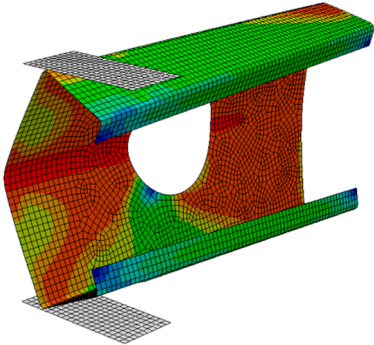
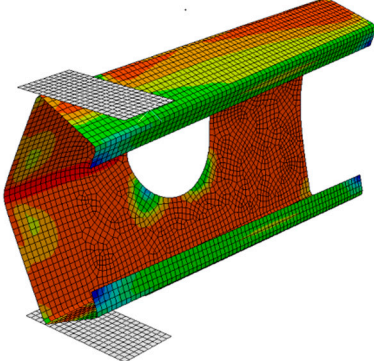
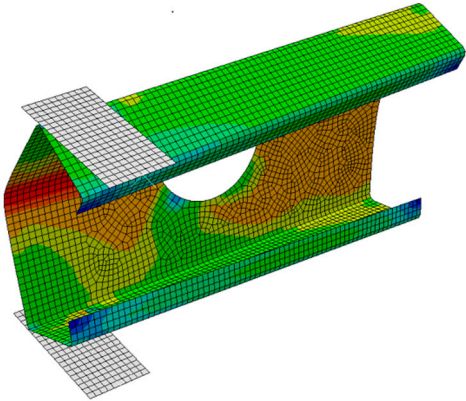
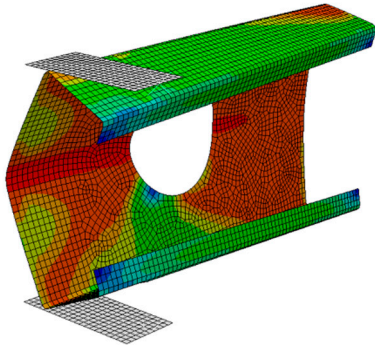
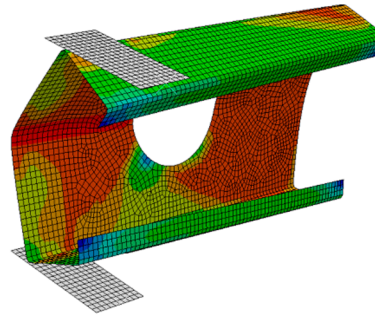
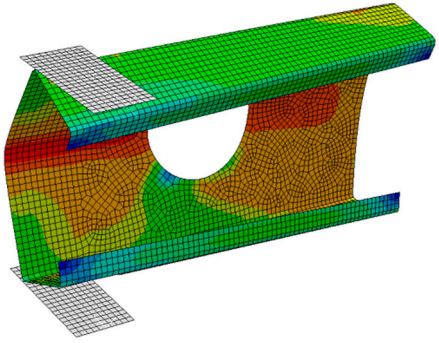
Duration of Heating	Exp	Water Cooled-ETF-without Hole	FEM
60 min		<p>S, Mises SNEG, (fraction = -1.0) (Avg: 75%)</p> <ul style="list-style-type: none"> <li>+1.451e+02</li> <li>+1.338e+02</li> <li>+1.225e+02</li> <li>+1.113e+02</li> <li>+1.000e+02</li> <li>+8.874e+01</li> <li>+7.747e+01</li> <li>+6.621e+01</li> <li>+5.494e+01</li> <li>+4.367e+01</li> <li>+3.240e+01</li> <li>+2.114e+01</li> <li>+9.870e+00</li> </ul>	
120 min		<p>S, Mises SNEG, (fraction = -1.0) (Avg: 75%)</p> <ul style="list-style-type: none"> <li>+8.868e+01</li> <li>+7.509e+01</li> <li>+6.829e+01</li> <li>+6.150e+01</li> <li>+5.470e+01</li> <li>+4.791e+01</li> <li>+4.111e+01</li> <li>+3.433e+01</li> <li>+2.752e+01</li> <li>+2.073e+01</li> <li>+1.393e+01</li> <li>+7.136e+00</li> </ul>	
Duration of Heating	Exp	Air-Cooled-ETF with Circular Hole	FEM
Reference		<p>S, Mises SNEG, (fraction = -1.0) (Avg: 75%)</p> <ul style="list-style-type: none"> <li>+3.426e+02</li> <li>+3.160e+02</li> <li>+2.895e+02</li> <li>+2.630e+02</li> <li>+2.364e+02</li> <li>+2.099e+02</li> <li>+1.834e+02</li> <li>+1.569e+02</li> <li>+1.303e+02</li> <li>+1.038e+02</li> <li>+7.728e+01</li> <li>+5.075e+01</li> <li>+2.422e+01</li> </ul>	
60 min		<p>S, Mises SNEG, (fraction = -1.0) (Avg: 75%)</p> <ul style="list-style-type: none"> <li>+2.045e+02</li> <li>+1.892e+02</li> <li>+1.738e+02</li> <li>+1.584e+02</li> <li>+1.430e+02</li> <li>+1.276e+02</li> <li>+1.122e+02</li> <li>+9.684e+01</li> <li>+8.145e+01</li> <li>+6.607e+01</li> <li>+5.068e+01</li> <li>+3.530e+01</li> <li>+1.991e+01</li> </ul>	

Table 3. Cont.

Duration of Heating	Exp	Air-Cooled-ETF with Circular Hole	FEM
120 min		<p>S, Mises SNEG, (fraction = -1.0) (Avg: 75%)</p> <ul style="list-style-type: none"> <li>+9.352e+01</li> <li>+8.527e+01</li> <li>+7.902e+01</li> <li>+7.176e+01</li> <li>+6.451e+01</li> <li>+5.726e+01</li> <li>+5.000e+01</li> <li>+4.275e+01</li> <li>+3.550e+01</li> <li>+2.824e+01</li> <li>+2.099e+01</li> <li>+1.374e+01</li> <li>+6.483e+00</li> </ul>	
Duration of Heating	Exp	Water-Cooled-ETF with Circular Hole	FEM
Reference		<p>S, Mises SNEG, (fraction = -1.0) (Avg: 75%)</p> <ul style="list-style-type: none"> <li>+3.426e+02</li> <li>+3.160e+02</li> <li>+2.895e+02</li> <li>+2.630e+02</li> <li>+2.364e+02</li> <li>+2.099e+02</li> <li>+1.834e+02</li> <li>+1.569e+02</li> <li>+1.303e+02</li> <li>+1.038e+02</li> <li>+7.728e+01</li> <li>+5.075e+01</li> <li>+2.422e+01</li> </ul>	
60 min		<p>S, Mises SNEG, (fraction = -1.0) (Avg: 75%)</p> <ul style="list-style-type: none"> <li>+1.883e+02</li> <li>+1.738e+02</li> <li>+1.593e+02</li> <li>+1.448e+02</li> <li>+1.303e+02</li> <li>+1.159e+02</li> <li>+1.014e+02</li> <li>+8.691e+01</li> <li>+7.242e+01</li> <li>+5.794e+01</li> <li>+4.346e+01</li> <li>+2.898e+01</li> <li>+1.450e+01</li> </ul>	
120 min		<p>S, Mises SNEG, (fraction = -1.0) (Avg: 75%)</p> <ul style="list-style-type: none"> <li>+9.038e+01</li> <li>+8.336e+01</li> <li>+7.634e+01</li> <li>+6.932e+01</li> <li>+6.229e+01</li> <li>+5.527e+01</li> <li>+4.825e+01</li> <li>+4.122e+01</li> <li>+3.420e+01</li> <li>+2.718e+01</li> <li>+2.016e+01</li> <li>+1.313e+01</li> <li>+6.110e+00</li> </ul>	

**Table 4.** View of failure mode images under ITF loads (Experiment vs. FEM).

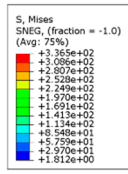
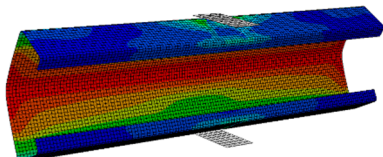
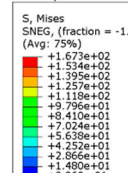
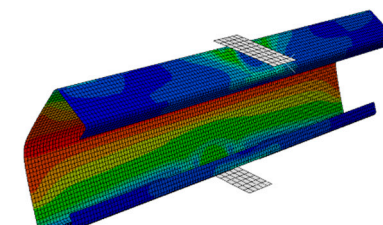
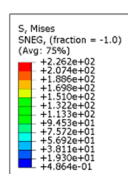
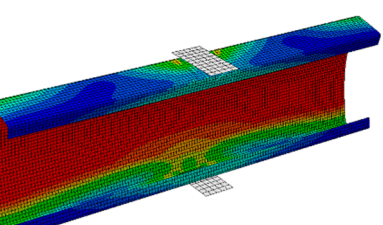
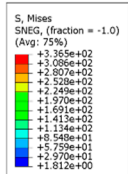
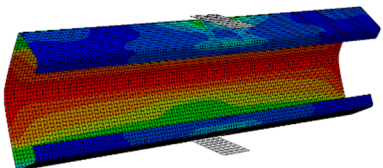
Duration of Heating	Exp	Air-Cooled-ITF without Hole	FEM
Reference			
60 min			
120 min			
Duration of Heating	Exp	Water-Cooled-ITF without Hole	FEM
Reference			

Table 4. Cont.

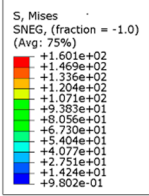
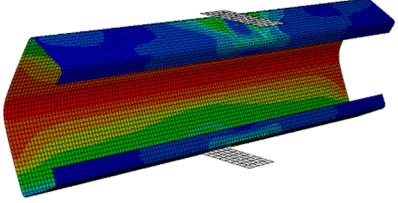
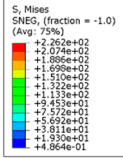
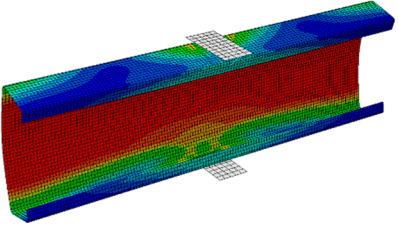
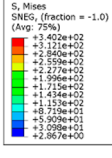
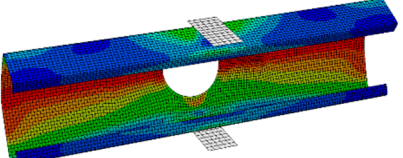
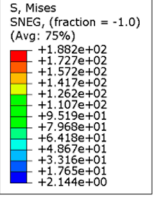
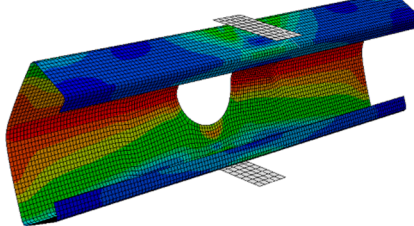
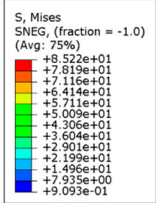
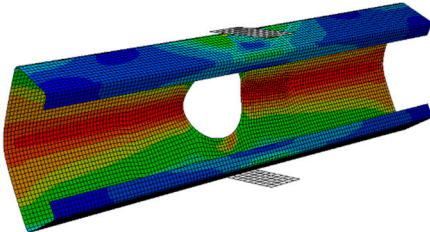
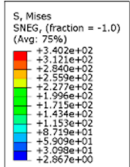
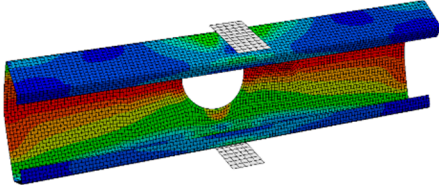
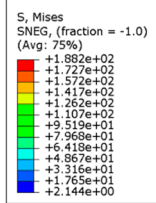
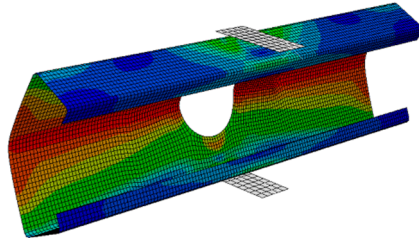
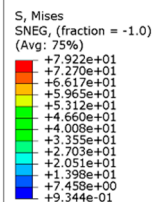
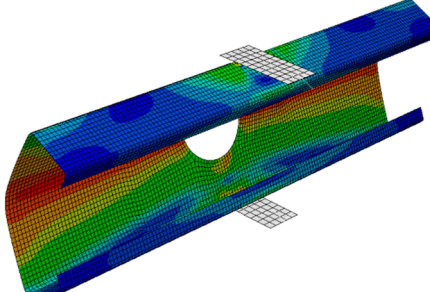
Duration of Heating	Exp	Water-Cooled-ITF without Hole	FEM
60 min			
120 min			
Duration of Heating	Exp	Air-Cooled-ITF with Circular Hole	FEM
Reference			
60 min			

Table 4. Cont.

Duration of Heating	Exp	Air-Cooled-ITF with Circular Hole	FEM
120 min			
Duration of Heating	Exp	Water-Cooled-ITF with Circular Hole	FEM
Reference			
60 min			
120 min			

### 5. Conclusions

This study explored the web-crippling capacities of high-performance cold-formed steel-lipped C-sections exposed to elevated temperatures subjected to different cooling (air-cooled and water-cooled) conditions by experimental as well as finite element modelling under ETF- and ITF-loading conditions. A total of 52 specimens were heated as per

ISO 834 fire curve at different durations of heating (30 min, 60 min, 90 min, and 120 min) and tested for web-crippling capacities. The effect of web opening on web-crippling capacities for both ETF and ITF was considered in the present study. The load-deflection behaviour and failure modes at different loading conditions were determined experimentally and compared with FEM.

- In the case of the ETF-loading condition, without considering the effect of web hole, the water-cooled specimens showed a decrease in web-crippling capacity of about 7.5–10% when compared to air-cooled specimens. When web hole is considered, under ETF loading condition, the decrease in strength was observed between 7.5 and 15%.
- At prolonged duration of heating, i.e., at 60 min and 120 min, the decrease in residual strength was observed as 37.2% to 71.44% for WH and 36.27% to 85.38% for WCH under ETF conditions.
- An increase in lateral deflection was observed at higher duration of heating for water-cooled specimens when compared to air-cooled specimens.
- In the case of ITF-loading conditions, about 10–15% increase in strength was inferred when compared to ETF-loading conditions.
- The failure modes and web-crippling capacity of FEM for both ETF and ITF were validated with experimental results and the capacity was found to be conservative.

#### 6. Scope for the Future Study

- Shear and web-crippling capacity of high-performance CFS specimens to be evaluated with edge stiffened and unstiffened conditions under the exposure of elevated temperature.
- To conduct a detailed parametric study on influencing parameters and proposal of new design guidelines for high-performance CFS structures under fire conditions.

**Author Contributions:** G.J. and T.K.: Investigation, Methodology, Formal analysis, Writing—original draft. A.N.: Resources, Supervised the research as well as the analysis of results. G.J., T.K. and A.N.: Project administration, Visualization, T.K., T.P.S. and M.E.M.: Funding, Numerical modelling, Data analysis, Writing—review and editing A.N., M.A. and A.R.D.: Validation suggested and chose the journal for submission. A.N., M.A. and A.R.D.: Collaborated, Writing—review and editing Coordinated the research, Reviewed for submission. All authors have read and agreed to the published version of the manuscript.

**Funding:** This research received no external funding.

**Informed Consent Statement:** Not applicable.

**Data Availability Statement:** The data presented in this study are available on request from the corresponding author.

**Conflicts of Interest:** This manuscript has not been submitted to, nor is it under review by, another journal or other publishing venue. The authors have no affiliation with any organization with a direct or indirect financial interest in the subject matter discussed in the manuscript. The authors declare no conflict of interest.

#### Abbreviations

CFS	Cold-Formed Steel
ETF	End Two Flange
ITF	Interior Two Flange
WH	Without Circular Hole
WCH	With Circular Hole
FEM	Finite Element Modelling

## References

1. Jaya Kumar, G.; Kiran, T.; Anand, N.; Al-Jabri, K. Influence of fire-resistant coating on the physical characteristics and residual mechanical properties of E350 steel section exposed to elevated temperature. *J. Struct. Fire Eng.* **2023**, *14*, 228–253. [[CrossRef](#)]
2. Jaya Kumar, G.; Kiran, T.; Anand, N.; Anbarasu, M.; Lubloy, E. Post-fire flexural behaviour and performance of unrestrained cold-formed steel built-up section beams: Experimental and numerical investigation. *Case Stud. Constr. Mater.* **2023**, *18*, e01978. [[CrossRef](#)]
3. McIntosh, A.; Kanthasamy, E.; Poologanathan, K.; Gunalan, S.; Gatheeshgar, P.; Corradi, M.; Higgins, C. Web crippling design of channel beams: Carbon steel, stainless steel and aluminium. *J. Constr. Steel Res.* **2022**, *196*, 107427. [[CrossRef](#)]
4. Sundararajah, L.; Mahendran, M.; Keerthan, P. Experimental studies of lipped channel beams subject to web crippling under two-flange load cases. *J. Struct. Eng.* **2016**, *142*, 04016058. [[CrossRef](#)]
5. Chen, B.; Roy, K.; Fang, Z.; Uzzaman, A.; Chi, Y.; Lim, J.B. Web crippling capacity of fastened cold-formed steel channels with edge-stiffened web holes, un-stiffened web holes and plain webs under two-flange loading. *Thin-Walled Struct.* **2021**, *163*, 107666. [[CrossRef](#)]
6. Degtyareva, N.; Poologanathan, K.; Mahendran, M. Web crippling tests of cold-formed steel channels with staggered web perforations. *Thin-Walled Struct.* **2021**, *159*, 107314. [[CrossRef](#)]
7. Sundararajah, L.; Mahendran, M.; Keerthan, P. Web crippling experiments of high strength lipped channel beams under one-flange loading. *J. Constr. Steel Res.* **2017**, *138*, 851–866. [[CrossRef](#)]
8. Kanthasamy, E.; Chandramohan, D.L.; Shanmuganathan, G.; Poologanathan, K.; Gatheeshgar, P.; Corradi, M.; McIntosh, A. Web crippling behaviour of cold-formed high-strength steel unlipped channel beams under End-One-Flange load case. *Case Stud. Constr. Mater.* **2022**, *16*, e01022. [[CrossRef](#)]
9. Fang, Z.; Roy, K.; Uzzaman, A.; Lim, J.B. Numerical simulation and proposed design rules of cold-formed stainless-steel channels with web holes under interior-one-flange loading. *Eng. Struct.* **2022**, *252*, 113566. [[CrossRef](#)]
10. Hancock, G.J.; Pham, C.H. Buckling Analysis of thin-walled sections under localised loading using the semi-analytical finite strip method. *Thin-Walled Struct.* **2015**, *86*, 35–46. [[CrossRef](#)]
11. Nguyen, V.V.; Hancock, G.J.; Pham, C.H. Analyses of thin-walled sections under localised loading for General End Boundary Conditions—Part 1: Pre-Buckling. *Thin-Walled Struct.* **2017**, *119*, 956–972. [[CrossRef](#)]
12. Nguyen, V.V.; Hancock, G.J.; Pham, C.H. Analyses of thin-walled sections under localised loading for General End Boundary Conditions—Part 2: Buckling. *Thin-Walled Struct.* **2017**, *119*, 973–987. [[CrossRef](#)]
13. *AISI S100*; North American Specification for the Design of Cold-Formed Steel Structural Members. American Iron and Steel Institute: Washington, DC, USA, 2016.
14. *AS/NZS 4600*; Australian/New Zealand Standard Cold-Formed Steel Structures. Standards Australia: Sydney, Australia, 2018.
15. *EN 1993-1-3*; Eurocode 3: Design of Steel Structures—Part 1–3: General Rules—Supplementary Rules for Cold-formed Members and Sheeting. National Standards Authority of Ireland: Dublin, Ireland, 2006.
16. Nguyen, V.V.; Hancock, G.J.; Pham, C.H. New Developments in the Direct Strength Method (DSM) for the design of Cold-Formed Steel Sections under localised loading. *Steel Constr.* **2017**, *10*, 227–233. [[CrossRef](#)]
17. Nguyen, V.V.; Hancock, G.J.; Pham, C.H. Consistent and Simplified DSM for Design of Cold-Formed Steel Structural Members under Localized Loading. *J. Struct. Eng.* **2020**, *146*, 04020090. [[CrossRef](#)]
18. Johnston, R.P.; Sonebi, M.; Lim, J.B.; Armstrong, C.G.; Wrzesien, A.M.; Abdelal, G.; Hu, Y. The collapse behaviour of cold-formed steel portal frames at elevated temperatures. *J. Struct. Fire Eng.* **2015**, *6*, 77–102. [[CrossRef](#)]
19. Roy, K.; Lim, J.B.; Lau, H.H.; Yong, P.M.; Clifton, G.C.; Johnston, R.P.; Wrzesien, A.; Mei, C.C. Collapse behaviour of a fire engineering designed single-storey cold-formed steel building in severe fires. *Thin-Walled Struct.* **2019**, *142*, 340–357. [[CrossRef](#)]
20. Nadjai, A.; Naveed, A.; Charlier, M.; Vassart, O.; Welsh, S.; Glorieux, A.; Sjoström, J. Large scale fire test: The development of a travelling fire in open ventilation conditions and its influence on the surrounding steel structure. *Fire Saf. J.* **2022**, *130*, 103575. [[CrossRef](#)]
21. Javed, M.F.; Hafizah, N.; Memon, S.A.; Jameel, M.; Aslam, M. Recent research on cold-formed steel beams and columns subjected to elevated temperature: A review. *Constr. Build. Mat.* **2017**, *144*, 686–701. [[CrossRef](#)]
22. Cai, Y.; Wang, L.; Zhou, F. Lean duplex stainless steel tubular sections undergoing web crippling at elevated temperatures. *J. Constr. Steel Res.* **2021**, *182*, 106681. [[CrossRef](#)]
23. Laim, L.; Rodrigues, J.P.C.; Da Silva, L.S. Experimental and numerical analysis on the structural behaviour of cold-formed steel beams. *Thin-Walled Struct.* **2013**, *72*, 1–13. [[CrossRef](#)]
24. Kiran, T.; Anand, N.; Mathews, M.E.; Andrushia, A.D.; Walls, R.; Kanagaraj, B. Post-fire behaviour and improving the performance of hot rolled open sections subjected to standard fire exposure. *Case Stud. Constr. Mater.* **2022**, *16*, e01021. [[CrossRef](#)]
25. Fang, Z.; Roy, K.; Lakshmanan, D.; Pranomrum, P.; Li, F.; Lau, H.H.; Lim, J.B. Structural behaviour of back-to-back cold-formed steel channel sections with web openings under axial compression at elevated temperatures. *J. Build. Eng.* **2022**, *54*, 104512. [[CrossRef](#)]
26. Li, H.T.; Young, B. Cold-formed high strength steel SHS and RHS beams at elevated temperatures. *J. Constr. Steel Res.* **2019**, *158*, 475–485. [[CrossRef](#)]
27. Lu, J.; Liu, H.; Chen, Z.; Luke, B. Experimental investigation of the residual mechanical properties of cast steels after exposure to elevated temperature. *Constr. Build. Mat.* **2017**, *143*, 259–271. [[CrossRef](#)]

28. Chong Ren; Liusi Dai; Yun'er Huang; Wenfu He, Experimental investigation of post-fire mechanical properties of Q235 cold-formed steel. *Thin-Walled Struct.* **2020**, *150*, 106651. [[CrossRef](#)]
29. *AISI S909-13*; Standard Test Method for Determining the Web Crippling Strength of Cold-Formed Steel Beams. American Iron and Steel Institute Specification (AISI): Washington, DC, USA, 2013.
30. *ISO 834-1*; Fire-Resistance Tests—Elements of Building Construction—Part 1: General Requirements. ISO Stand.: Geneva, Switzerland, 1999.
31. *ASTM E8/E8M-16*; Standard Test Methods for Tension Testing of Metallic Materials. ASTM International: West Conshohocken, PA, USA, 2016.
32. ABAQUS/Standard Version 6. 13, *ABAQUS/CAE User's Manual*; Dassault Systèmes Simulia Corp.: Providence, RI, USA, 2013.

**Disclaimer/Publisher's Note:** The statements, opinions and data contained in all publications are solely those of the individual author(s) and contributor(s) and not of MDPI and/or the editor(s). MDPI and/or the editor(s) disclaim responsibility for any injury to people or property resulting from any ideas, methods, instructions or products referred to in the content.